# One-Step Synthesis of Bifunctional Nickel Phosphide Nanowires as Electrocatalysts for Hydrogen and Oxygen Evolution Reactions

Dong Xiang[1], Biao Zhang[1]*, Hongsheng Zhang[1] and Liangping Shen[2,3]*

[1]School of Mechatronics Engineering, Harbin Institute of Technology, Harbin, China, [2]Hubei Yangtze Memory Labs, Hubei University, Wuhan, China, [3]Hubei Key Laboratory of Ferro and Piezoelectric Materials and Devices, School of Microelectronics, Hubei University, Wuhan, China

The $Ni_2P$ nanowires were simply synthesized *via* a rapid one-step hydrothermal approach, in which deionized water, red phosphorus, nickel acetate, and hexadecyl trimethyl ammonium bromide were used as the solvent, phosphor and nickel sources, and active agent, respectively. The as-synthesized $Ni_2P$ nanowire clusters were composed of uniform nanowires with length of about 10 μm and diameter of about 40 nm. The $Ni_2P$ nanowires exhibited enhanced electrocatalytic activity for both hydrogen evolution reaction and oxygen evolution reaction This work provides good guidance for the rational design of nickel phosphides with unique nanostructures for highly efficient overall water splitting.

**Keywords: nickel phosphide, nanowire, hydrogen evolution reaction, oxygen evolution reaction, hydrothermal**

## INTRODUCTION

Growing energy demands and worsening environmental issues have motivated a large amount of research into developing efficient energy conversion/storage systems for sustainable alternatives (Tan et al., 2020; Ji et al., 2021), e.g., Li-ion batteries (Chen et al., 2016; Zhang et al., 2017a; Li et al., 2017), supercapacitor (Wang et al., 2020; Zhao et al., 2021), water splitting (Wang et al., 2016a; Wang et al., 2016b; Swierk and Mallouk, 2017), and fuel cells (Debe, 2012). Hydrogen generated by water splitting is one of the key strategies for conquering these energy challenges (Kuang et al., 2017). However, the half-reactions of water-splitting, namely hydrogen evolution reaction (HER) and oxygen evolution reaction (OER), suffer from high overpotentials due to sluggish electrode kinetics (Huang et al., 2017). Efficient electrocatalysts, such as noble metal catalysts Pt, Ru, and Ir, are one of the core parts to improve the efficiency of the water decomposition process (Zhou et al., 2016; Zhang et al., 2017b). However, the high cost and scarcity of resources have severely restricted their large-scale applications. Hence, it is fairly urgent to explore efficient, low-cost, and earth-abundant non-noble bifunctional electrocatalysts for HER and OER.

In recent years, nickel-based compounds [oxide (Gong et al., 2014; Qiu et al., 2017; Zhang et al., 2018), hydroxide (Danilovic et al., 2012; Rao et al., 2016), sulfide (Feng et al., 2015; Zhu et al., 2016), and phosphide (Gan et al., 2020; Ji et al., 2021)] have displayed remarkable electrocatalytic activity and stability toward OER and HER, as bifunctional electrocatalysts (Vij et al., 2017). Among them, nickel phosphides could be considered as an efficient and promising candidate in numerous fields of electrochemistry including catalysis (Rao et al., 2016), lithium-ion batteries (Li et al., 2016a), and supercapacitors (Wan et al., 2017). Of note, nickel phosphides (especially metallic-phased phosphide, such as $Ni_2P$) are excellent catalysts for HER and OER due to their unique

physicochemical properties imparting their high-efficiency and low overpotential (Feng et al., 2014; Liao and Huang, 2017). For example, Matthias Dries et al. (Menezes et al., 2016) reported two remarkably active nickel phosphides that delivered an overpotential of 295 mV for $Ni_{12}P_5$ and 330 mV for $Ni_2P$ at 10 mA cm$^{-2}$ for HER, and realized a low potential of 1.64 and 1.58 V at 10 mA cm$^{-2}$ for OER in 1 M KOH, respectively. $Ni_xP_y$ nanocatalysts are highly efficient at driving an overpotential of 1.57 V at 10 mA cm$^{-2}$ in 1.0 M KOH for OER (Li et al., 2016b). $Ni_2P$ nanoparticles exhibit an overpotential of 0.2 V at 10 mA cm$^{-2}$ in 0.1 M KOH for HER (Li et al., 2015). It is reported that another kind of $Ni_2P$ nanoparticle delivers an overpotential of 290 mV at 10 mA cm$^{-2}$ in 1 M KOH (Stern et al., 2015). However, the preparation approaches of metal phosphide special nanostructures mainly relies on the high-temperature (over 300°C) oil phase method, e.g., $Ni_{12}P_5$, $Ni_2P$, and $Ni_5P_4$ nanocrystals (320°C) (Pan et al., 2015), and two-step high-temperature (over 300°C) gas–solid reaction, such as CoP nanoneedle (Wang et al., 2016c), CoP film (450°C) (Hellstern et al., 2016), porous $Ni_2P$ (500°C) (Wang et al., 2016d), FeP nanorods (500°C) (Xiong et al., 2016), and Ni-P porous nanoplates (300°C) (Yu et al., 2016). The low-energy consumption preparations of nickel phosphides with special nanostructures are rarely reported and hard to control, restraining the practical applications of nickel phosphides in electrocatalysis.

The special microstructures of nanowire clusters play a significant role in promoting catalytic activity because of their abundant edge active sites and facilitated charge (including electrons and ions) transfer path (Sivanantham et al., 2016; Tang et al., 2016). In this work, we report a facile one-pot synthesis of $Ni_2P$ nanowire clusters using the hydrothermal method and the as-prepared $Ni_2P$ nanowires exhibit enhanced electrocatalytic activity for both HER and OER.

## EXPERIMENTAL SECTION

### Preparation of $Ni_2P$ nanowires

In a typical experiment, 2 mmol $Ni(CH_3COO)_2 \cdot 4H_2O$, 9 mmol red phosphorus, and 1 mmol hexadecyl trimethyl ammonium Bromide (CTAB) were dissolved in 60 ml pure water. Then, the above solution was transferred into a 100 ml Teflon-lined stainless autoclave, and heated at 195°C for 30 h. After cooling to room temperature, the collected precipitate was filtered and washed with water and ethanol, and then dried overnight.

### Materials Characterization

X-ray diffraction (XRD) patterns of the samples were analyzed by Philips X'Pert PRO (Cu Kα, λ = 0.1542 nm). The microstructures of the samples were examined by scanning electron microscope (SEM, FEI Quanta 200) and the refined microstructures were probed by transmission electron microscopy (TEM, Philips, Tecnai G20). X-ray photoelectron spectroscopy (XPS) spectra were collected on a Kratos AXIS Ultra DLD-600W XPS (a monochromatic Al Kα (1,486.6 eV) as X-ray source).
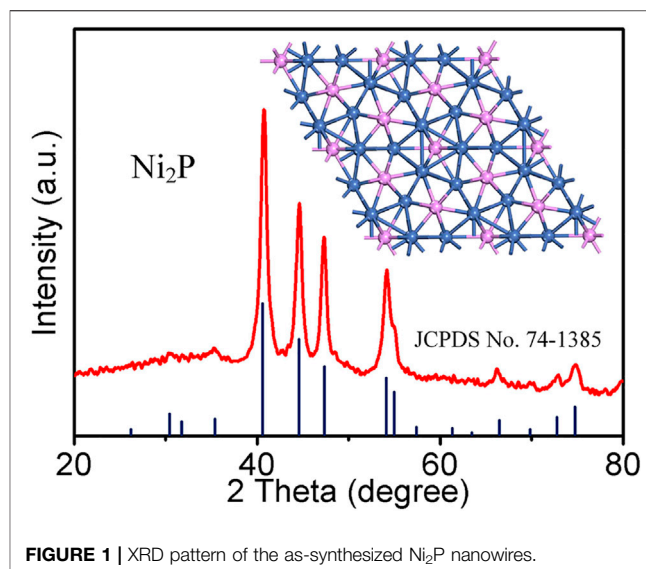


**FIGURE 1** | XRD pattern of the as-synthesized $Ni_2P$ nanowires.

## Electrochemical Measurement

For the preparation of the working electrode, 5 mg electrocatalyst and 1 mg Ketjen black were dispersed in 968 μL of water/ethanol (volume ratio 4:1) mixture with addition of 32 μL Nafion solution (5 wt%). After ultrasonic dispersion for 30 min, 4 μL of the slurry was drop-cast onto a glassy carbon (GC) electrode with a diameter of 5 mm. The HER and OER tests were carried out by electrochemical workstation (CHI760E, Shanghai Chenhua) and Pine Modulated Speed Rotator with Pt silk as the counter electrode and Ag/AgCl as reference electrode. The polarization curves for HER and OER were obtained at a scan rate of 5 mV s$^{-1}$ under a rotation rate of 1,600 rpm in N$_2$-saturated 1 M KOH solution. Electrochemical impedance spectroscopy (EIS) test was performed from a frequency range of 10 kHz to 0.01 Hz at a voltage of −0.4 V (vs. RHE) for HER.

## RESULTS AND DISCUSSION

The crystal structure of the as-prepared $Ni_2P$ was examined by XRD (**Figure 1**). The diffraction peaks are observed at 30.5, 31.8, 35.3, 40.7, 44.6, 47.4, 54.2, 55.0, 66.4, 72.7, and 74.8°, corresponding to planes (110), (101), (200), (111), (201), (210), (300), (211), (310), (311), and (400). The sample collected at 30 h can be indexed to the hexagonal phase of $Ni_2P$ (JCPDS 74-1,385) with P-62m space group (the inset in **Figure 1** in the atomic structure). There is no superfluous peak, indicating the successful synthesis of pure $Ni_2P$.

The nanostructures of obtained $Ni_2P$ nanowires were characterized by SEM and TEM. **Figures 2A,B** reveal that the $Ni_2P$ sample is composed of uniform nanowire clusters with lengths of about 10 μm and diameters of about 100 nm. Meanwhile, the orientation of most nanowires is in the same direction as in Figure 2A, and there are numerous hump-like particles on the surface of the nanowires in **Figure 2B**, exposing a large number of active sites during the electrocatalysis process. A
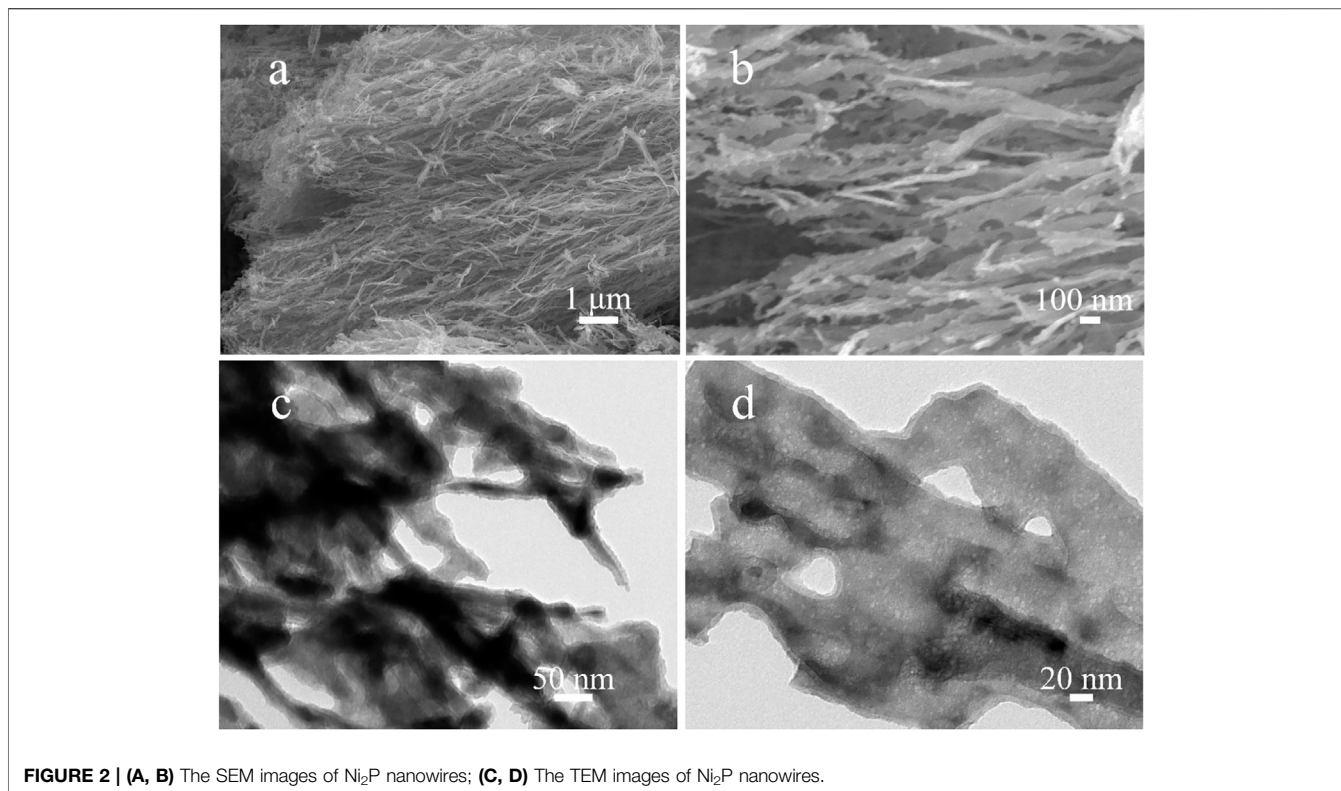
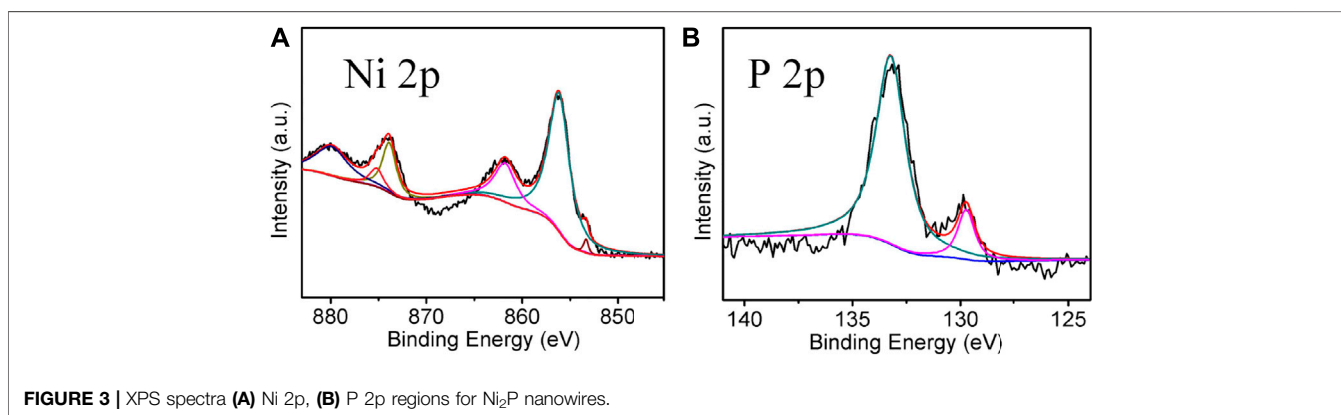**FIGURE 2 |** **(A, B)** The SEM images of Ni$_2$P nanowires; **(C, D)** The TEM images of Ni$_2$P nanowires.



**FIGURE 3 |** XPS spectra **(A)** Ni 2p, **(B)** P 2p regions for Ni$_2$P nanowires.

TEM image in **Figure 2C** shows uniform nanowires of the Ni$_2$P sample, and the inside of the nanowires reveals a large number of nanosized holes from the highly magnified TEM image in **Figure 2D**.

**Figures 3A,B** show the core-level XPS spectra of Ni and P elements of Ni$_2$P, respectively. As presented, the peaks located at 853.4, 856.3, and 861.9 eV are associated with Ni 2p$_{3/2}$. The peak at 853.6 eV revealed that Ni species in Ni$_2$P have a very small positive charge, while the peak at 129.7 eV for P 2p indicates Ni$_2$P has a very small negative charge (Wan et al., 2017). In addition, the peaks at 856.3 and 861.9 eV in Ni 2p$_{3/2}$ and the peak at 133.3 eV in P 2p are likely to be ascribed to nickel phosphate formed on the surface of Ni$_2$P due to the exposure of the sample to air (Xiao et al., 2016).

In order to explore the formation mechanism of Ni$_2$P nanowires, a series of samples that underwent different reaction times were collected. The SEM images of the sample collected at 3 h in **Figures 4A,D** show the surface of a block has a uniform arrangement of projections with a length of about 200 nm and a diameter of about 40 nm. The sample obtained at 7 h shows a larger cavity than that at 3 h as shown in **Figures 4B,E**. **Figures 4C,F** reveal that the sample obtained at 30 h is composed of nanowire clusters with the same orientation and length of about 10 μm and a diameter of about 100 nm. Taking red phosphorus as the phosphorus source and nickel acetate as the nickel source during hydrothermal reaction, the Ni$_2$P nanowires were successfully synthesized. At first, red phosphorus is difficult to dissolve in deionized water. With the
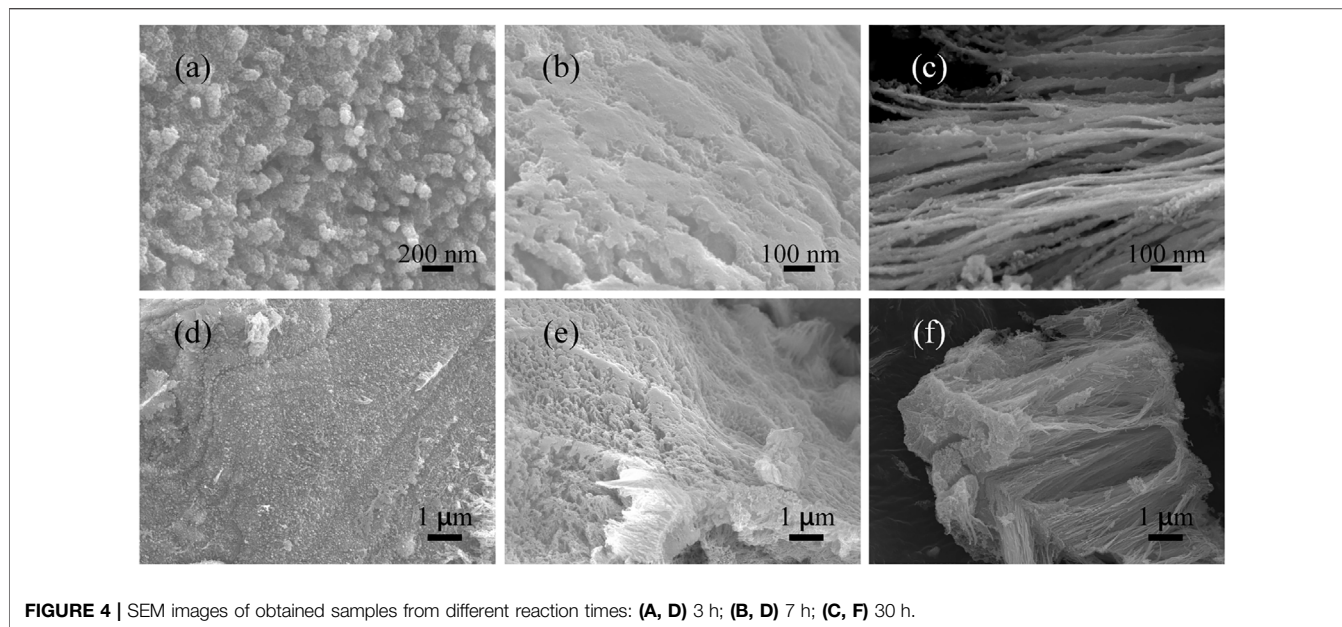
**FIGURE 4 |** SEM images of obtained samples from different reaction times: **(A, D)** 3 h; **(B, D)** 7 h; **(C, F)** 30 h.
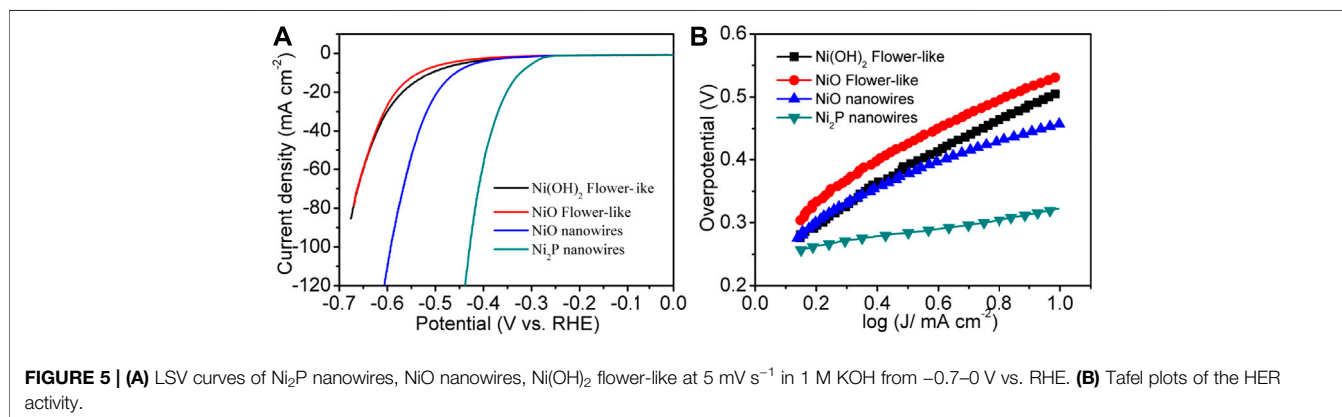


**FIGURE 5 | (A)** LSV curves of $Ni_2P$ nanowires, NiO nanowires, $Ni(OH)_2$ flower-like at 5 mV s$^{-1}$ in 1 M KOH from −0.7–0 V vs. RHE. **(B)** Tafel plots of the HER activity.

hydrothermal process (process 1), red phosphorus was gradually decomposed to generate phosphine, and then the phosphine reacted with nickel ions in solution and nucleation occurs at the surface of the block. Following this (process 2), the block of red phosphorus was gradually consumed, and the nanowires gradually increase. Finally (process 3), the $Ni_2P$ nanowires were formed, accompanied with red phosphorus and nickel ions depleting.

**Figure 5A** shows the linear sweep voltammogram (LSV) curve of $Ni_2P$ nanowire catalysts at 5 mV s$^{-1}$ after 20 cycles of cyclic voltammogram (50 mV s$^{-1}$) activation. For comparative analysis, the LSV curves of the samples, *i.e.*, $Ni_2P$ nanowires, $Ni(OH)_2$ flower-like nanostructures, and NiO flower-like nanostructures (SEM images as shown in **Supplementary Figure S1**), were also measured at 5 mV s$^{-1}$ with the same mass loadings of 0.175 mg cm$^{-2}$. The polarization curves of $Ni_2P$ nanowires exhibit a remarkable electrocatalytic activity for HER with a small onset potential and overpotential (η) to reach a current density of 10 mA cm$^{-2}$. The ranking of the overpotentials for

those catalysts is: $Ni_2P$ nanowires (320 mV) < $Ni_2P$ nanowires (458 mV) < $Ni(OH)_2$ nanoflowers (512 mV) < NiO nanoflowers (535 mV). It is clear that $Ni_2P$ nanowires exhibit the highest electrocatalytic activity toward HER. The Tafel slope for the $Ni_2P$ nanowires catalyst was about 73 mV dec$^{-1}$ (**Figure 5B**), much smaller than those of the NiO nanowires (157 mV dec$^{-1}$), flower-like $Ni(OH)_2$ (234 mV dec$^{-1}$), and flower-like NiO (213 mV dec$^{-1}$), which further confirmed the superior electrocatalytic HER kinetics of $Ni_2P$ nanowires.

To further understand the reason for the excellent electrocatalytic HER activity of $Ni_2P$ nanowires, EIS analysis was carried out (**Figure 6**). The charge transfer resistance under high frequency of $Ni_2P$ nanowire is low, which further implies its higher conductivity. The lower charge transfer resistance and higher diffusion of electrolyte ions indicate good electronic conductivity and high OH$^-$ ion transfer speed in the interface of active materials/electrolyte. The aforesaid electrochemical performances reveal that $Ni_2P$ nanowire clusters are an efficient and sturdy electrocatalyst for HER in strongly basic media.
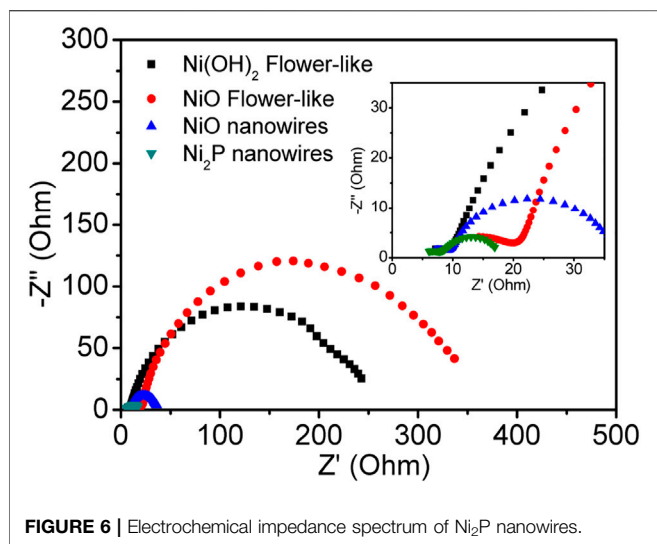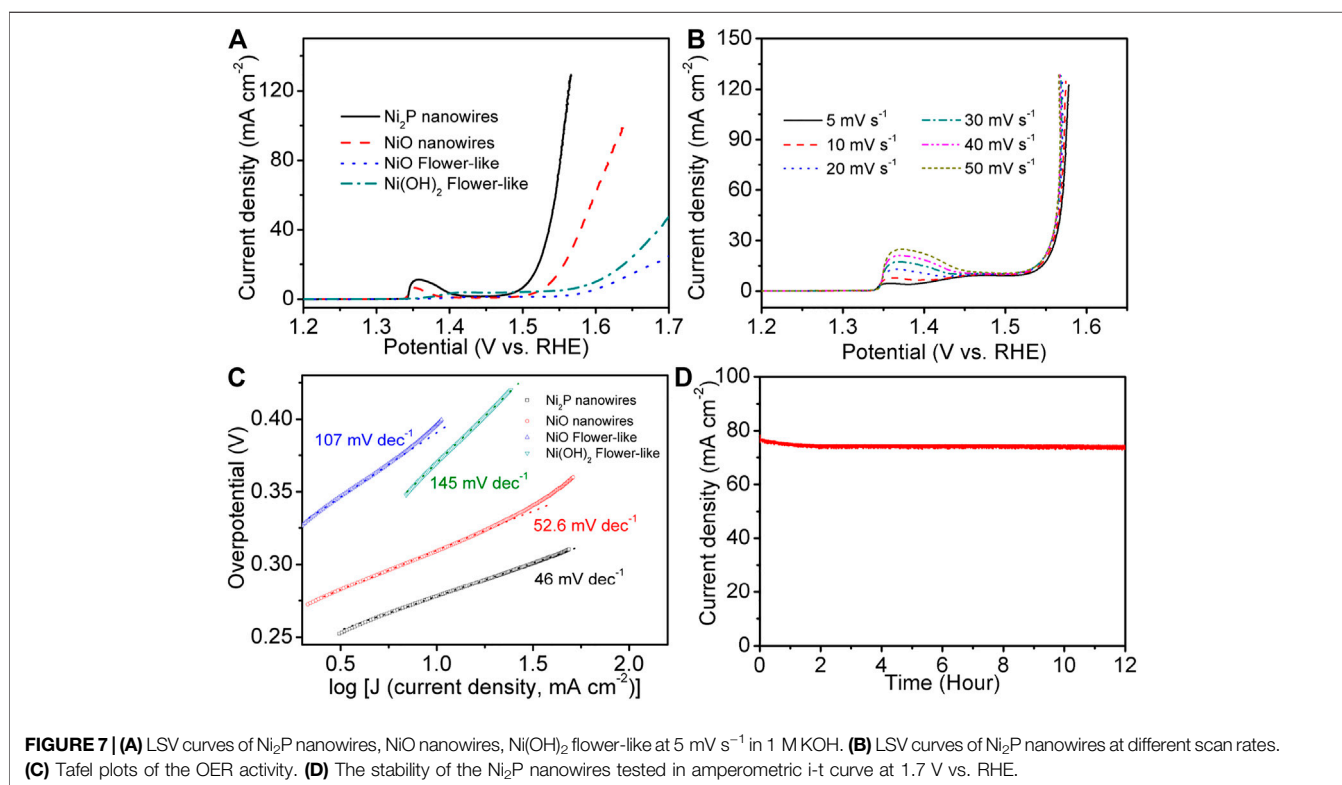
**FIGURE 6** | Electrochemical impedance spectrum of Ni$_2$P nanowires.

**Figure 7A** shows the linear sweep voltammograms (LSV) curve of Ni$_2$P nanowire catalyst at 5 mV s$^{-1}$ after 20 cycles of cyclic voltammogram (at the scan rate of 50 mV s$^{-1}$) activation. For comparative analysis, the LSV curves of NiO nanowires, Ni(OH)$_2$ flower-like, and NiO flower-like catalysts were also measured at 5 mV s$^{-1}$ with the same mass loadings of 0.175 mg cm$^{-2}$. The polarization curves of Ni$_2$P nanowires exhibit a higher current density and more negative OER overpotential of 280 mV than those of NiO nanowires (310 mV), Ni(OH)$_2$ flower-like (370 mV), and NiO flower-like (390 mV). In order to further study the polarization property, the

LSV curves of Ni$_2$P nanowires at different scan rates were displayed in **Figure 7B**. It indicates that the polarization curves have no difference in addition to the intensity of the oxidation peaks. This oxidation peak is also reversible for Ni$_2$P nanowires as observed from the cyclic voltammogram (**Supplementary Figure S2**). The Tafel slope for the Ni$_2$P nanowires catalyst was about 46 mV dec$^{-1}$ (**Figure 7C**), much smaller than those of the NiO nanowires (52.6 mV dec$^{-1}$), flower-like Ni(OH)$_2$ (145 mV dec$^{-1}$), and flower-like NiO (107 mV dec$^{-1}$), which further confirmed the superior electrocatalytic OER kinetics of Ni$_2$P nanowires. The stability of the Ni$_2$P nanowires for OER was tested in amperometric i-t curve at 1.7 V (vs. RHE) for 12 h (**Figure 7D**), indicating its good durability.

## CONCLUSION

In summary, we firstly synthesized Ni$_2$P nanowires using a facile one-step hydrothermal approach. The as-synthesized Ni$_2$P is composed of nanowire clusters with a uniform length of about 10 μm and a diameter of about 40 nm. There are a large number of nanoparticles on the surface of the nanowires, providing a large number of active sites during the electrocatalysis process. The overpotential of Ni$_2$P nanowires is 320 mV and clearly demonstrates the Tafel slope of 73 mV dec$^{-1}$ for HER. Meanwhile, the Ni$_2$P nanowires show excellent electrocatalytic OER activity with overpotential of 1.51 V (vs. RHE) and Tafel slope of 46 mV dec$^{-1}$. This work provides good guidance for the rational design of nickel phosphides with unique nanostructures for highly efficient overall water splitting.



**FIGURE 7** | **(A)** LSV curves of Ni$_2$P nanowires, NiO nanowires, Ni(OH)$_2$ flower-like at 5 mV s$^{-1}$ in 1 M KOH. **(B)** LSV curves of Ni$_2$P nanowires at different scan rates. **(C)** Tafel plots of the OER activity. **(D)** The stability of the Ni$_2$P nanowires tested in amperometric i-t curve at 1.7 V vs. RHE.

# DATA AVAILABILITY STATEMENT

The raw data supporting the conclusion of this article will be made available by the authors, without undue reservation.

# AUTHOR CONTRIBUTIONS

All authors listed have made a substantial, direct, and intellectual contribution to the work and approved it for publication.

# FUNDING

# SUPPLEMENTARY MATERIAL

The Supplementary Material for this article can be found online at: https://www.frontiersin.org/articles/10.3389/fchem.2021.773018/full#supplementary-material

# REFERENCES

Chen, Y., Fu, K., Zhu, S., Luo, W., Wang, Y., Li, Y., et al. (2016). Reduced Graphene Oxide Films with Ultrahigh Conductivity as Li-Ion Battery Current Collectors. *Nano Lett.* 16, 3616–3623. doi:10.1021/acs.nanolett.6b00743

Danilovic, N., Subbaraman, R., Strmcnik, D., Chang, K.-C., Paulikas, A. P., Stamenkovic, V. R., et al. (2012). Enhancing the Alkaline Hydrogen Evolution Reaction Activity through the Bifunctionality of Ni(OH)2/Metal Catalysts. *Angew. Chem. Int. Ed.* 51, 12495–12498. doi:10.1002/anie.201204842

Debe, M. K. (2012). Electrocatalyst Approaches and Challenges for Automotive Fuel Cells. *Nature* 486, 43–51. doi:10.1038/nature11115

Feng, L.-L., Yu, G., Wu, Y., Li, G.-D., Li, H., Sun, Y., et al. (2015). High-Index Faceted Ni3S2 Nanosheet Arrays as Highly Active and Ultrastable Electrocatalysts for Water Splitting. *J. Am. Chem. Soc.* 137, 14023–14026. doi:10.1021/jacs.5b08186

Feng, L., Vrubel, H., Bensimon, M., and Hu, X. (2014). Easily-prepared dinickel phosphide (Ni2P) nanoparticles as an efficient and robust electrocatalyst for hydrogen evolution. *Phys. Chem. Chem. Phys.* 16, 5917–5921. doi:10.1039/c4cp00482e

Gan, Y., Wang, C., Chen, X., Liang, P., Wan, H., Liu, X., et al. (2020). High conductivity Ni12P5 nanowires as high-rate electrode material for battery-supercapacitor hybrid devices. *Chem. Eng. J.* 392, 123661. doi:10.1016/j.cej.2019.123661

Gong, M., Zhou, W., Tsai, M.-C., Zhou, J., Guan, M., Lin, M.-C., et al. (2014). Nanoscale Nickel Oxide/Nickel Heterostructures for Active Hydrogen Evolution Electrocatalysis. *Nat. Commun.* 5, 4695. doi:10.1038/ncomms5695

Hellstern, T. R., Benck, J. D., Kibsgaard, J., Hahn, C., and Jaramillo, T. F. (2016). Engineering Cobalt Phosphide (CoP) Thin Film Catalysts for Enhanced Hydrogen Evolution Activity on Silicon Photocathodes. *Adv. Energ. Mater.* 6, 1501758. doi:10.1002/aenm.201501758

Huang, H., Yu, C., Zhao, C., Han, X., Yang, J., Liu, Z., et al. (2017). Iron-tuned Super Nickel Phosphide Microstructures with High Activity for Electrochemical Overall Water Splitting. *Nano Energy* 34, 472–480. doi:10.1016/j.nanoen.2017.03.016

Ji, J., Wan, H., Zhang, B., Wang, C., Gan, Y., Tan, Q., et al. (2021). Co 2+/3+/4+ -Regulated Electron State of Mn-O for Superb Aqueous Zinc-Manganese Oxide Batteries. *Adv. Energ. Mater.* 11 (6), 2003203. doi:10.1002/aenm.202003203

Kuang, P., Tong, T., Fan, K., and Yu, J. (2017). In Situ Fabrication of Ni-Mo Bimetal Sulfide Hybrid as an Efficient Electrocatalyst for Hydrogen Evolution over a Wide pH Range. *ACS Catal.* 7, 6179–6187. doi:10.1021/acscatal.7b02225

Li, H., Wang, W., Gong, Z., Yu, Y., Piao, l., Chen, H., et al. (2015). Shape-controlled Synthesis of Nickel Phosphide Nanocrystals and Their Application as Hydrogen Evolution Reaction Catalyst. *J. Phys. Chem. Sol.* 80, 22–25. doi:10.1016/j.jpcs.2014.12.013

Li, J., Li, J., Zhou, X., Xia, Z., Gao, W., Ma, Y., et al. (2016). Highly Efficient and Robust Nickel Phosphides as Bifunctional Electrocatalysts for Overall Water-Splitting. *ACS Appl. Mater. Inter.* 8, 10826–10834. doi:10.1021/acsami.6b00731

Li, Q., Ma, J., Wang, H., Yang, X., Yuan, R., and Chai, Y. (2016). Interconnected Ni 2 P nanorods grown on nickel foam for binder free lithium ion batteries. *Electrochimica Acta* 213, 201–206. doi:10.1016/j.electacta.2016.07.105

Li, T., Xu, Y., Xing, F., Cao, X., Bian, J., Wang, N., et al. (2017). Boosting Photoelectrochemical Water Splitting by TENG-Charged Li-Ion Battery. *Adv. Energ. Mater.* 7, 1700124. doi:10.1002/aenm.201700124

Liao, W., and Huang, L. (2017). Improving the Oxygen Evolution Performance of Nickel Phosphide Nanoparticles with Satellite Nitrogen-doped Carbon Quantum Dots. *Mater. Lett.* 209, 106–110. doi:10.1016/j.matlet.2017.07.127

Menezes, P. W., Indra, A., Das, C., Walter, C., Göbel, C., Gutkin, V., et al. (2016). Uncovering the Nature of Active Species of Nickel Phosphide Catalysts in High-performance Electrochemical Overall Water Splitting. *ACS Catal.* 7, 103–109. doi:10.1021/acscatal.6b02666

Pan, Y., Liu, Y., Zhao, J., Yang, K., Liang, J., Liu, D., et al. (2015). Monodispersed Nickel Phosphide Nanocrystals with Different Phases: Synthesis, Characterization and Electrocatalytic Properties for Hydrogen Evolution. *J. Mater. Chem. A.* 3, 1656–1665. doi:10.1039/c4ta04867a

Qiu, Z., Ma, Y., Edström, K., Niklasson, G. A., and Edvinsson, T. (2017). Controlled Crystal Growth Orientation and Surface Charge Effects in Self-Assembled Nickel Oxide Nanoflakes and Their Activity for the Oxygen Evolution Reaction. *Int. J. Hydrogen Energ.* 42, 28397–28407. doi:10.1016/j.ijhydene.2017.09.117

Rao, Y., Wang, Y., Ning, H., Li, P., and Wu, M. (2016). Hydrotalcite-like Ni(OH)2 Nanosheets In Situ Grown on Nickel Foam for Overall Water Splitting. *ACS Appl. Mater. Inter.* 8, 33601–33607. doi:10.1021/acsami.6b11023

Sivanantham, A., Ganesan, P., and Shanmugam, S. (2016). Hierarchical NiCo2S4Nanowire Arrays Supported on Ni Foam: An Efficient and Durable Bifunctional Electrocatalyst for Oxygen and Hydrogen Evolution Reactions. *Adv. Funct. Mater.* 26, 4661–4672. doi:10.1002/adfm.201600566

Stern, L.-A., Feng, L., Song, F., and Hu, X. (2015). Ni2P as a Janus catalyst for water splitting: the oxygen evolution activity of Ni2P nanoparticles. *Energy Environ. Sci.* 8, 2347–2351. doi:10.1039/c5ee01155h

Swierk, J. R., and Mallouk, T. E. (2017). Correction: Design and Development of Photoanodes for Water-Splitting Dye-Sensitized Photoelectrochemical Cells. *Chem. Soc. Rev.* 46, 559. doi:10.1039/c6cs90124g

Tan, Q., Li, X., Zhang, B., Chen, X., Tian, Y., Wan, H., et al. (2020). Valence Engineering via In Situ Carbon Reduction on Octahedron Sites Mn 3 O 4 for Ultra-Long Cycle Life Aqueous Zn-Ion Battery. *Adv. Energ. Mater.* 10 (38), 2001050. doi:10.1002/aenm.202001050

Tang, C., Gan, L., Zhang, R., Lu, W., Jiang, X., Asiri, A. M., et al. (2016). Ternary FexCo1-xP Nanowire Array as a Robust Hydrogen Evolution Reaction Electrocatalyst with Pt-like Activity: Experimental and Theoretical Insight. *Nano Lett.* 16, 6617–6621. doi:10.1021/acs.nanolett.6b03332

Vij, V., Sultan, S., Harzandi, A. M., Meena, A., Tiwari, J. N., Lee, W.-G., et al. (2017). Nickel-Based Electrocatalysts for Energy-Related Applications: Oxygen Reduction, Oxygen Evolution, and Hydrogen Evolution Reactions. *ACS Catal.* 7, 7196–7225. doi:10.1021/acscatal.7b01800

Wan, H., Li, L., Chen, Y., Gong, J., Duan, M., Liu, C., et al. (2017). One pot synthesis of Ni 12 P 5 hollow nanocapsules as efficient electrode materials for oxygen evolution reactions and supercapacitor applications. *Electrochimica Acta* 229, 380–386. doi:10.1016/j.electacta.2017.01.169

Wang, C., Song, Z., Wan, H., Chen, X., Tan, Q., Gan, Y., et al. (2020). Ni-Co Selenide Nanowires Supported on Conductive Wearable Textile as Cathode for Flexible Battery-Supercapacitor Hybrid Devices. *Chem. Eng. J.* 400, 125955. doi:10.1016/j.cej.2020.125955

Wang, J., Cui, W., Liu, Q., Xing, Z., Asiri, A. M., and Sun, X. (2016). Recent Progress in Cobalt-Based Heterogeneous Catalysts for Electrochemical Water Splitting. *Adv. Mater.* 28, 215–230. doi:10.1002/adma.201502696

Wang, P., Song, F., Amal, R., Ng, Y. H., and Hu, X. (2016). Efficient Water Splitting Catalyzed by Cobalt Phosphide-based Nanoneedle Arrays Supported on Carbon Cloth. *ChemSusChem* 9, 472–477. doi:10.1002/cssc.201501599

Wang, Q., Hisatomi, T., Jia, Q., Tokudome, H., Zhong, M., Wang, C., et al. (2016). Scalable water splitting on particulate photocatalyst sheets with a solar-to-hydrogen energy conversion efficiency exceeding 1%. *Nat. Mater* 15, 611–615. doi:10.1038/nmat4589

Wang, X., Li, W., Xiong, D., and Liu, L. (2016). Fast Fabrication of Self-supported Porous Nickel Phosphide Foam for Efficient, Durable Oxygen Evolution and Overall Water Splitting. *J. Mater. Chem. A.* 4, 5639–5646. doi:10.1039/c5ta10317g

Xiao, J., Lv, Q., Zhang, Y., Zhang, Z., and Wang, S. (2016). One-step Synthesis of Nickel Phosphide Nanowire Array Supported on Nickel Foam with Enhanced Electrocatalytic Water Splitting Performance. *RSC Adv.* 6, 107859–107864. doi:10.1039/c6ra20737e

Xiong, D., Wang, X., Li, W., and Liu, L. (2016). Facile Synthesis of Iron Phosphide Nanorods for Efficient and Durable Electrochemical Oxygen Evolution. *Chem. Commun.* 52, 8711–8714. doi:10.1039/c6cc04151e

Yu, X.-Y., Feng, Y., Guan, B., Lou, X. W., and Paik, U. (2016). Carbon Coated Porous Nickel Phosphides Nanoplates for Highly Efficient Oxygen Evolution Reaction. *Energ. Environ. Sci.* 9, 1246–1250. doi:10.1039/c6ee00100a

Zhang, C., Park, S.-H., O'Brien, S. E., Seral-Ascaso, A., Liang, M., Hanlon, D., et al. (2017). Liquid Exfoliation of Interlayer Spacing-Tunable 2D Vanadium Oxide Nanosheets: High Capacity and Rate Handling Li-ion Battery Cathodes. *Nano Energy* 39, 151–161. doi:10.1016/j.nanoen.2017.06.044

Zhang, L., Xiao, J., Wang, H., and Shao, M. (2017). Carbon-Based Electrocatalysts for Hydrogen and Oxygen Evolution Reactions. *ACS Catal.* 7, 7855–7865. doi:10.1021/acscatal.7b02718

Zhang, T., Wu, M.-Y., Yan, D.-Y., Mao, J., Liu, H., Hu, W.-B., et al. (2018). Engineering Oxygen Vacancy on NiO Nanorod Arrays for Alkaline Hydrogen Evolution. *Nano Energy* 43, 103–109. doi:10.1016/j.nanoen.2017.11.015

Zhao, X., Wan, H., Liang, P., Wang, N., Wang, C., Gan, Y., et al. (2021). Favorable anion adsorption/desorption of high rate NiSe2 nanosheets/hollow mesoporous carbon for battery-supercapacitor hybrid devices. *Nano Res.* 14, 2574–2583. doi:10.1007/s12274-020-3257-z

Zhou, X., Jin, J., Zhu, X., Huang, J., Yu, J., Wong, W.-Y., et al. (2016). New Co(OH)2/CdS nanowires for efficient visible light photocatalytic hydrogen production. *J. Mater. Chem. A.* 4, 5282–5287. doi:10.1039/c6ta00325g

Zhu, T., Zhu, L., Wang, J., and Ho, G. W. (2016). *In Situ* chemical etching of tunable 3D Ni3S2 superstructures for bifunctional electrocatalysts for overall water splitting. *J. Mater. Chem. A.* 4, 13916–13922. doi:10.1039/c6ta05618k